A Unique Sub-micron Scanning System use for CMOS APS crosstalk characterization

Igor Shcherback, Boris Belotserkovsky, Alex Belenky, Orly Yadid-Pecht

The VLSI Systems Center
Ben Gurion University
P.O.B. 653 Beer-Sheva 84105, ISRAEL
Tel: 972-8-6461512
Fax: 972-8-6477620
E-Mail: oyp@ee.bgu.ac.il

ABSTRACT

This paper presents the pioneer use of our unique Sub-micron Scanning System (SSS) for point spread function (PSF) and crosstalk (CTK) measurements of focal plane CMOS Active Pixel Sensor (APS) arrays. The system enables the combination of near-field optical and atomic force microscopy measurements with the standard electronic analysis. This SSS enables full PSF extraction for imagers via sub-micron spot light stimulation. This is unique to our system. Other systems provide Modulation Transfer Function (MTF) measurements, and cannot acquire the true PSF, therefore limiting the evaluation of the sensor and its performance grading. A full PSF is required for better knowledge of the sensor and its specific faults, and for research – to enable better optimization of pixel design and imager performance.
In this work based on the thorough scanning of different "L" shaped active area pixel designs (the responsivity variation measurements on a subpixel scale) the full PSF was obtained and the crosstalk distributions of the different APS arrays are calculated. The obtained PSF points out the pronounced asymmetry of the diffusion within the array, mostly caused by the certain pixel architecture and the pixels arrangement within the array. We show that a reliable estimate of the CTK in the imager is possible; the PSF use for the CTK measurements enables not only its magnitude determination (that can be done by regular optical measurements), but also to discover its main causes, enabling the design optimization per each potential pixel application.

Keywords: CMOS Active Pixel Sensor (APS), Point spread Function (PSF), Modulation Transfer Function (MTF), crosstalk (CTK), diffusion process, modeling.

INTRODUCTION

Past several years of intensive work[1-10], have made APS imagers be considered a viable alternative to CCDs in many application fields. However, investigations have still to be performed for improving APS performance in order to meet dedicated application requirements and to provide designers with better control. It appears as important to acquire experimental data concerning parameters affecting electro-optics performance, mostly responsivity and crosstalk. The aims of the presented work are: verification of the sub-micron scanning system applicability for the diffusion/crosstalk measurements of focal plane CMOS APS arrays. The work is based on experimental data acquired from several APS chips fabricated in a standard 0.5µm CMOS technology process. Identical topologies of the photosensitive area have been implemented. All the pixels share a common, traditional three-transistor type readout circuitry. The measurements (the responsivity variation on a subpixel scale) will be described here thoroughly.
In CMOS APS arrays, the pixel area is constructed of two functional parts (see Fig. 1). The first part, that has a certain geometrical shape, is the sensing element itself: the active area (which consist of photodiode in a silicon substrate) that absorbs the illumination energy within it and turns that energy into charge carriers. Each imaging site has a depletion region of several micrometers near the silicon surface. Any photocarrier generated in this depletion region is collected at this imaging site (we assume perfect collection efficiency for carriers at or within the depletion region). The second part is the control circuitry required for readout of this charge. The ratio between the active area and the total pixel area is

referred as the Fill Factor (FF), which in APS is less than 100 percent (in contrast to CCDs where the FF can approach 100%).

Fig. 1.

Photon absorption in the silicon depends on the absorption coefficient α, which is a function of the wavelength. Blue light, with wavelength $\lambda \approx 0.4\mu m$, is strongly absorbed in the first few micrometers of silicon, since α is large in this spectral region. Longer wavelengths, $\lambda \approx 0.6\mu m$, for instance, have a smaller absorption coefficient, which means more of the photocarriers can be generated outside the depletion regions. These carriers diffuse to the original imaging site or to a nearby site where they are collected, before they are lost to a bulk recombination process. Electrical crosstalk is the phenomenon whereby photogenerated minority charge carriers generated within the nominal absorption/collection regions of a particular element of the pixel array undergo diffusion within the silicon substrate and are collected by a different element. The peripheral collection of photocarriers along the lateral edge of the photodiode is known as the peripheral photoresponse or the lateral photocurrent [11-14]. The effect of crosstalk (as the result of this diffusion) on the acquired image would be limited resolution, i.e., "sharp" edges would be "blurred".
The generated overall signal is proportional to the pixel geometry (i.e., the signal grows with photodiode dimensions increase) and could be presented as the sum of the main, i.e., the photodiode contribution itself, and the periphery contribution, due to the successfully collected diffusion carriers. Fig. 2 shows a schematic cross section of several imager sites, which indicates the depletion-region boundaries.

Fig. 2.

In the case of CMOS APS, its charge to voltage conversion gain is typically dominated by the junction capacitance of the photodiode itself, which is built up from the bottom and the side-wall capacitances.

$$C_{jdep} = \frac{C_{J0B} A_D}{\left[1 - \left(\frac{V_d}{\varphi_B}\right)\right]^{m_j}} + \frac{C_{J0sw} P_D}{\left[1 - \left(\frac{V_d}{\varphi_{Bsw}}\right)\right]^{m_{jsw}}} \qquad (1)$$

where
C_{jdep} - represents the depletion capacitance of the p-n junction,
C_{j0B} and C_{J0sw} - represents zero bias capacitances of the bottom and the side-wall components respectively,
V_d - is the voltage applied to the photodiode,
φ_B and φ_{Bsw} - stand for the build-in potential of the bottom and the side-walls respectively,
m_j and m_{jsw} -stand for the grading coefficients of the bottom and the side-walls respectively,
A_D - represents the photodiode area (bottom component),
P_D - represents the photodiode perimeter.

The conversion factor, $\mathrm{C_{gain}} = \frac{q_{el}}{C_{jdep}}$ [μVolt/e$^-$], is inversely proportional to the pixel geometry (q_{el} - is the electron charge).
Pixel signal output is proportional to the product of the integrated photocarriers and the conversion gain. However, the pixel photosignal dependence on its geometrical shape (the photodiode active area and perimeter) and fill factor, that has been represented in [15], enables behavior identification of different pixel types and quantifies the device geometry deviations effect on its overall performance. It indicates that for any potential pixel active area shape, a reliable estimate of the degradation of image performance is possible, so that the tradeoff between conflicting factors, such as integration photocarriers and conversion gain, could be compared per each pixel design for optimum overall sensor performance.

EXPERIMENTAL DETAILS

The SSS is able to hit onto a desirable point within the pixel (e.g., a well-defined point within the pixel region), after penetration through the certain oxide depth (e.g., 5-8 micron), with the desirable diameter size of the laser beam (e.g., ~0.5micron).
An optical spot of size $\approx 0.5\mu m$ was used to scan the APS over a single pixel and its immediate and second step neighbors in a raster fashion. The light is projected through the confocal fiber tip directly onto the sensor pixel. The tip allows the transmission of the light signal through the transparent oxide layers (of the certain depth, see Fig. 3) without beam broadening.

Fig. 3.

The data acquisition was taken at the particular pixel within a 70x70 um scanned area, i.e., only one pixel was read out at each point of the scan (see Fig. 4). The obtained signal as a function of the spot position provides a responsivity map of the scanned area that includes the pixel response and the crosstalk influences.

Fig. 4.

Assume only one pixel within the array is active. The "window region" i.e., the photodiode of the active pixel is the only region where the wide (nonzero bias) depletion layer exists and the photocarrier collection occurs. The incoming laser light generates (at a certain depth according to the exponential absorption law) electron-hole pairs i.e., minority charge carriers. Part of these carriers diffuse (with equal probability to all directions) directly to the depletion region, where they subsequently contribute to the resultant signal. Thereby, the resulting PSF we obtain in the "window" region (see Fig. 5) consist of the detection of those charge carriers, which successfully diffused to the depletion region. The value at each point represents the electrical outcome of the three-dimensional photocarrier diffusion (i.e., the integration over the depth at each point) from this point to the depletion. Thus, the 2D signal map plane we get in the experiment can be generally considered as a "diffusion map" of the 3D diffusion in the device.

Fig. 5.

A set of measurements for a number of randomly chosen chips was performed at the same conditions (including environment temperature). A similar sized area of $70\times70\ \mu m^2$ (pixel pitch is ~ $14\mu m$) was scanned with a $1\mu m$ resolution step*, in such a way that for each scan only one pixel from the inner subarray was chosen to be active. Note that the scanner spot size is small compared with the pixel size; therefore, the effects of the laser spot profile on the measured PSF are not considered. The obtained results, i.e., the electrical outcome, were integrated over the pixel area in order to obtain the resulting output signal for each of the scanned pixels (the active one and its nearest and second step neighbors). The obtained integration results were averaged for each scanned region and summarized for each chip. The CTK is determined thus as the ratio between the output of the active pixel and one of its neighbors. Based on the obtained PSF results the averaged CTK values are about 5.5% for the adjacent neighbor and 1.2% for the second neighbor. The summarized crosstalk results, their discussion and conclusions are presented herein.

CROSSTALK RESULTS AND DISCUSSION

The results show that there is essential difference in the overall CTK signal obtained from the neighbors, i.e., the distribution of the values for the adjacent pixels is as presented in Fig. 5; where numbers indicate the queue of the overall CTK signal results one relative to another, such that the signal value obtained from the right nearest neighbor is the highest one, the upper pixel shows the second result, etc.
We found and show here that the diffusion in general and the crosstalk in particular has a strong dependence on the particular pixel layout design.

---

* Since a metal layer covers the pixel non-active area and integration over the pixel area was used, a resolution step of $1\mu m$ is enough for CTK determination.

We make use of the fact that each one of the parameters determining the signal output depends on the photodiode area and perimeter [15]. The general expression for the output signal is:

$$\frac{V_{out}(\lambda)}{N_{p\lambda}} = (\text{integration photocarriers} \times \text{conversion gain}) = \frac{k_1 A + k_2 Pd\left(\frac{S-A}{S}\right)\left(1-\frac{4Pi-P}{8L_{diff}}\right)}{k_3 A + k_4 P} \qquad (2)$$

The left part of this equation, $\frac{V_{out}(\lambda)}{N_{p\lambda}}$, corresponds to the pixel output voltage signal related to the number of incoming photons (in a time unit). In the right part, $\frac{k_1 A + k_2 Pd\left(\frac{S-A}{S}\right)\left(1-\frac{4Pi-P}{8L_{diff}}\right)}{k_3 A + k_4 P}$, the denominator or, more precisely its inverse, represents the conversion factor, while the numerator represents the integrated photocarriers. The numerator consists of two parts, contributing to the total carriers number collected by the imager. The first part, $k_1 A$, represents the contribution of the photocarriers created within the photodiode itself, i.e., the "active area" contribution. The second part, $k_2 Pd\left(\frac{S-A}{S}\right)\left(1-\frac{4Pi-P}{8L_{diff}}\right)$- represents the "periphery" or the "lateral diffusion current" contribution, i.e., the carriers that were created within the photodiode surrounding and had successfully diffused and been collected by the photodiode.

$\frac{1}{k_3 A + k_4 P}$ - represents the conversion gain, that depends on both, the photodiode area and perimeter.

$Pd\ [\mu m^2]$ - represents the lateral collecting surface or interaction cross-section for lateral diffusion. Here $P[\mu m]$-is the photodiode perimeter, and $d\,[\mu m]$-is the junction depth. Since $\partial Px \ll Px$; $\partial Py \ll Py$ (∂Px; ∂Py - are the lateral depletion stretch of the photodiode), they can be neglected, and we can assume that the perimeter, $P[\mu m]$ itself defines the lateral interaction area boundary, see Fig. 6.

Fig. 6

$\left(\frac{S-A}{S}\right)$ [Dimensionless] - Since the optical generation rate is relatively uniform throughout the substrate, this multiplier is proportional to the relative number of carriers created within the pixel substrate around the photodiode. Here, $(S-A)[\mu m^2]$– represents the substrate, i.e., the unoccupied photodiode surroundings area within the pixel, whereas $A[\mu m^2]$- is the photodiode active area. The less the fill factor, the more the number of the carriers created within the photodiode surroundings, which can diffuse and contribute to the total signal.

It is obvious that this multiplier represents the array influence on the pixel photodiode, and the boundary condition, e.g., as the active area increases and reaches the pixel boundary (i.e., $A = S$, for all the pixels in array)—the diffusion contribution to the signal zeroes. Fig. 7 illustrates the situation where the diffusion equals zero as a result of the photodiode area extension for all pixels in the array. Thereby this multiplier represents the relative number of the potential diffusion contributors.

Fig. 7

$\left(1-\frac{4Pi-P}{8L_{diff}}\right)$[Dimensionless]- indicates the approximated distance that the prospective contributor has to pass before it is trapped. Fig. 8 shows a schematic cross section of several imager sites, which illustrates the diffusion distance dependence on the photodiode geometry. Here, $L_{diff}\left[mm\right]$-is the characteristic diffusion length, Pi – is the pixel pitch. As the photodiode dimensions, and its perimeter $P\left[mm\right]$ go up, the maximum distance that a carrier created within the substrate has to diffuse before it is collected by the peripheral side-wall collecting surface Pd decreases, so the diffusion contribution increases.

This multiplier is obtained from the series expansion of the expression $\exp\left(-\frac{4Pi-P}{8L_{diff}}\right)$, representing the one-dimensional diffusion equation solution. Since the distances between the photodiodes in the array, and therefore the maximum carrier path, are small compared to the minority carrier diffusion length, taking the first two terms is adequate.
All other affecting parameters are described herein.

Fig. 8.

$V_{out}\left(l\right)$ $\left[volt\right]$ - The pixel signal output for a particular wavelength.
N_{pl} $\left[Photons/\sec\right]$ - The photon irradiance. $k_1\left[mm^{-2}\right]$- A coefficient, which describes the unity “active area” contribution to the total number of electrons collected by the imager, i.e., the number of electrons collected by the unity photodiode area in a time unit. $k_2\left[mm^{-2}\right]$ - A coefficient, which describes the photodiode “peripheral unity area” contribution to the total number of electrons collected by the imager, i.e., the number of electrons collected by the “side-wall collecting surface” within the substrate depth. k_3, k_4 $\left[\text{aF}/mm^2, \text{aF}/mm\right]$ - Coefficients, which describe the bottom and side-wall capacities correspondingly in regular junction capacity meaning, as described in Eq. 1, and defined by the particular process data.
In summary, the diffusion contribution to the overall signal is proportional to the lateral collecting area, the number of possible contributors, and to the distance that the carrier has to pass before its collection by the photodiode.
In the simple case of the CTK measurements the output signal depends only on the diffusion contribution, in view of the fact that the readout pixel is not illuminated while CTK is measured from its neighbor.
The output signal (from the readout pixel) is proportional to the lateral collecting area, the number of possible contributors, and to the distance that the carrier has to pass before it is collected by the photodiode :

$$V_{out} \propto Pd \bullet (S-A) \bullet \left(\exp(-\frac{r}{L_{diff}})\right) \qquad (3)$$

Here, $\left(\exp(-\frac{r}{L_{diff}})\right)$ represents the approximated distance $r\left[mm\right]$ that the prospective contributor has to pass before it is trapped.
The obtained signal map enables easy determination of the distance from the depletion boundary (of the readout pixel) such that the signal value became 1/3e smaller than the value from the central pixel (the signal reduces tenfold regarding to the maximum level, and became comparable to the background level). This determines the enclosed area of which the diffusion carriers can contribute. In Fig. 9: (a) indicates the lateral distances, where the signal value reduces to 1/3e from its maximum value in relation to the central pixel, (b) represents the corresponding layout with the indication of the enclosed areas. The ratio between the output signals can be approximated as the ratio between the mentioned enclosed areas multiplied by the corresponding lateral collecting surfaces, i.e., Eq. 3 reduces to:

$$\frac{Vk_{out}(1)}{Vk_{out}(1)} = \left. \frac{\sum Pk_n Ak_n}{\sum Pk_n Ak_n} \right|_{\text{at the distance where the value is 1/3e of max}} \quad (4)$$

where V_{out} stays for the output signal, P - represents the lateral collecting surface length (the depletion depth is constant, regarding the cross-section), A – represents the enclosed area, i.e., the area that contributes the prospective carriers, k – represents the pixels contributing to the CTK in correspondence to Fig. 3; n – represents the amount of the collecting surfaces, e.g., for pixels "1" and "2" n=3, while for pixels "3" and "4" n=1. This expression makes use of the axiom of additivity of the antithetical events.

Fig. 9

Based on the above approximation and the layout data we obtain, for example, that the output signals ratio between "2" and "1" pixels $V1_{out} / V2_{out} = 1.387$, while the measurements result is ~1.39. . It should be noted that the surface leakage, and the non-ideal transmission rate of the overlayers are not included in the present analysis and are considered to be second order effects [16].

We affirm thus that the CTK present within the pixel array mostly caused by the certain pixel architecture and the pixels arrangement within the array. We therefore conclude that a reliable estimate of the CTK in the imager is possible; the proposed method based on the SSS exploitation and the PSF use for the CTK measurements enables not only its magnitude determination (that can be done by regular optical measurements), but also to discover its main causes, enabling the design optimization per each potential pixel application.

SUMMARY

This work introduces a way for CMOS photodiode crosstalk determination and prediction based on the submicron scanning system and the CMOS APS photosignal model use. The CTK dependence on the pixel geometrical shape (the photodiode active area and perimeter) and the pixels arrangement within the array has been shown. This result brings out clearly the possibility of a design enabling minimum CTK extraction, and thus can be used as a predictive tool for design optimization.

The proposed model is process dependent, and further research is required for a process-based model [17,18]. In addition, since this is the first model giving a quantitative value to the substrate influence, further model enhancements are expected to follow.

ACKNOWLEDGEMENTS

The authors would like to thank the Israeli Ministry of Trade for supporting this project.

REFERENCES

[1] J. Hynecek, "BCMD-An improved photosite structure for high-density image sensors," IEEE Trans. Electron Devices, vol.38, ED -5, pp. 1011-1020, May 1991.

[2] K. Matsumoto, I. Takayanagi, T. Nakamura, R. Ohta, "The operation mechanism of a charge modulation device (CMD) image sensor," IEEE Trans. Electron Devices, vol. 38, ED -5, pp. 989-998, May 1991.

[3] O. Yadid-Pecht, R. Ginosar and Y. Shacham-Diamand, "A random access photodiode array for intelligent image capture," IEEE Trans. Electron Devices, vol. 38, no. 8, pp. 1772 - 1781, Aug.1991.

[4] E. R. Fossum, "CMOS Image Sensors: Electronic Camera on A Chip," IEEE Trans. Electron Devices, vol. 44, pp. 1689-1698, Oct 1997.

[5] O. Yadid-Pecht, B. Mansoorian, E. Fossum, B. Pain, "Optimization of active pixel sensor noise and responsivity for scientific applications," Proc. SPIE/IS&T Sym. on Electronic Imaging: Science and Technology, San Jose, California, Feb. 1997.

[6] Mendis, S Kemeny, R Gee, B. Pain, C. Staller, Q. Kim and E. Fossum, “CMOS active pixel image sensors for highly integrated imaging systems,” IEEE J. Solid State Circuits, vol. 32, pp. 187-197, Feb. 1997.

[7] P. Magnan, A. Gautrand, Y. Degerli, C. Marques, F. Lavernhe, C. Cavadore, F. Corbiere,J. Farre, O. Saint-Pe, M. Tulet, R. Davancens, “Influence of pixel topology on performances of CMOS APS imagers,” Proc. SPIE, vol. 3965, 2000.

[8] J. Bogaerts, B. Dierickx, “Total dose effects on CMOS Active Pixel Sensors,” Proc. SPIE, vol. 3965, pp. 157-167, 2000.

[9] H. Tian, B. Fowler, A. El-Gamal, “Analysis of temporal noise in CMOS photodiode active pixel sensor,” IEEE J. Solid State Circuits, vol. 36, pp. 92-100, Jan. 2001.

[10] H. Tian, X. Liu, S.H. Lim, S. Kleinfelder, A. El-Gamal, “Active pixel sensors fabricated in a standard 0.18um CMOS technology,” Proc. SPIE, vol. 4306, pp. 441-449, 2001.

[11] J. P. Lavine, E. A. Trabka, B. C. Burkey, T. J. Tredwell, E. T. Nelson, C. N. Anagnosyopoulos, “ Steady-State Photocarrier Collection in Silicon Imaging Devices,” IEEE Trans. Electron Devices, vol. 30, ED-9, pp. 1123-1134, Sept. 1983.

[12] D. Kavaldjiev, Z. Ninkov, “Subpixel Sensitivity Map for a Charge Coupled Device sensor,” Optical Engineering, vol. 37, no. 3, pp. 948-954, Mar. 1998.

[13] J. S. Lee, R. I. Hornsey, “Photoresponse of photodiode arrays for solid-state image sensors,” J. Vacuum Science & Tech., vol. 18, no 2, pp. 621-625, March 2000.

[14] I. Shcherback, O. Yadid-Pecht, “CMOS APS MTF Modeling,” IEEE Trans. Electron Devices, vol. 48, ED-12, pp. 2710-2715, Dec. 2001.

[15] I. Shcherback, O. Yadid-Pecht,” Photoresponse analysis and pixel shape optimization for CMOS Active Pixel Sensors,” accepted for publication IEEE Trans. Electron Devices, special issue on Image Sensors, Jan. 2003.

[16] D. Ramey, J. T. Boyd, “Computer Simulation of Optical Crosstalk in Linear Imaging Arrays,” J. Quant. Electron, vol. 17, pp. 553-556, Apr. 1981.

[17] H. Wong, “Technology and device Scaling Considerations for CMOS Imagers,” IEEE Trans. Electron Devices, vol. 43, ED-12, pp. 2131-2142, Dec. 1996.

[18] T. Lule, S. Benthien, H. Keller, F. Mutze, P. Rieve, K. Seibel, M. Sommer, M. Bohm, “Sensitivity of CMOS based imagers and scaling perspectives,” IEEE Trans. Electron Devices, vol. 47, ED-11, pp. 2710-2122, Nov. 2000.

LIST OF FIGURES

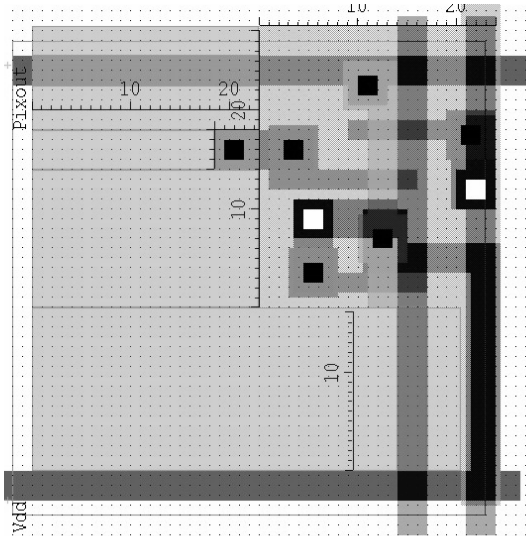

Fig. 1. Layout example of an L-shaped active area pixel design. The geometrical dimensions are indicated.

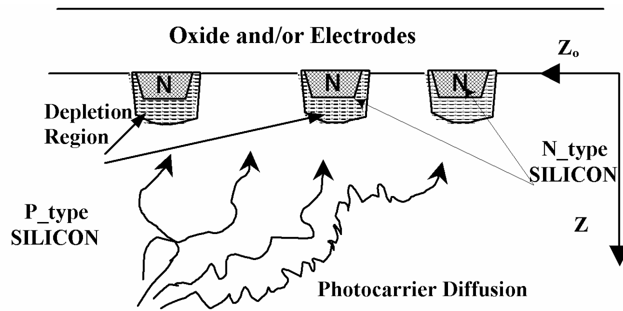

Fig. 2: Schematic cross-section of several imager sites, with indication of the depletion-region boundaries.

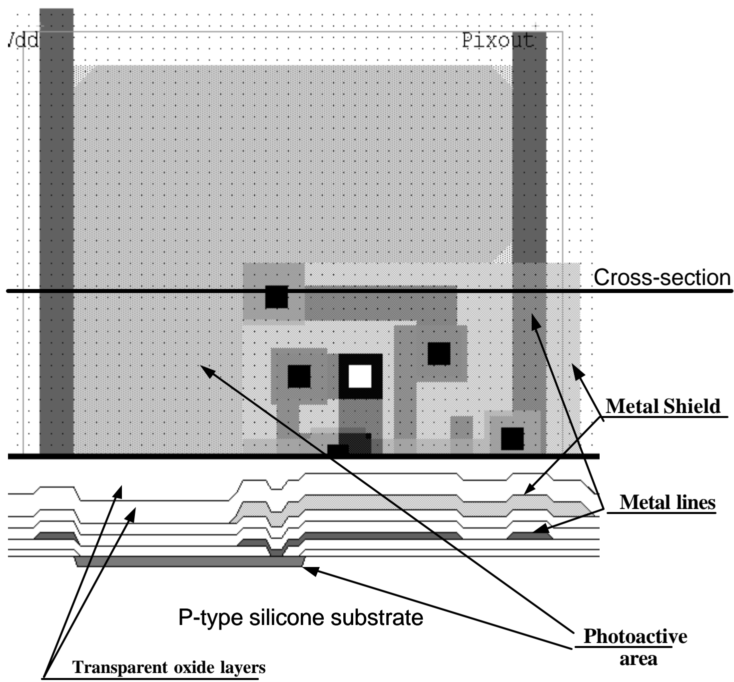

Fig. 3. Basic pixel layout /cross-section

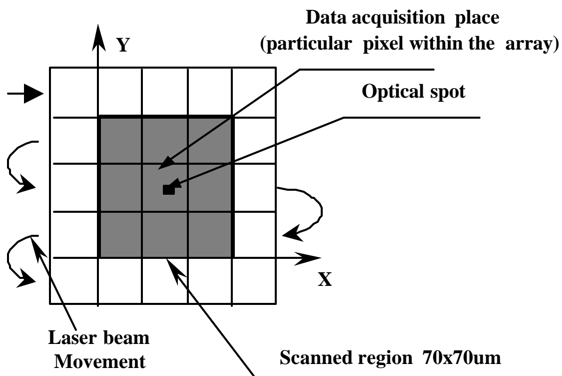

Fig. 4. Experiment description. The solid squares represent the APS array. The optical spot (dark filled rectangle) is scanned over the array in a raster fashion within the scanned region (dashed line rectangle).

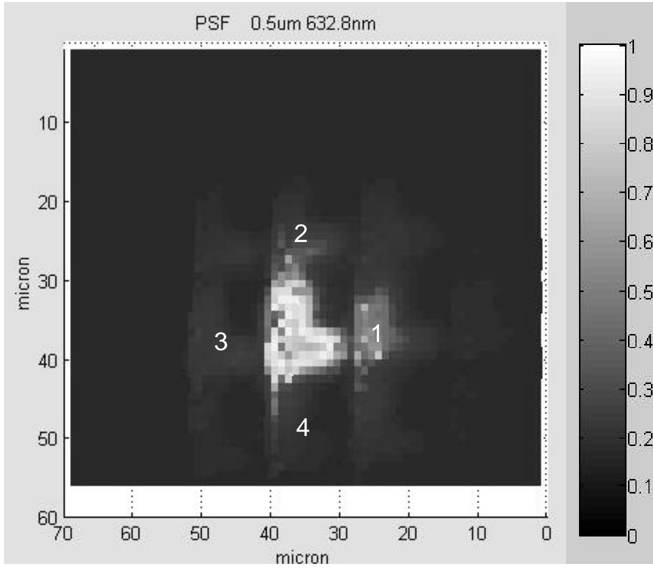

Fig. 5. Plot example of an actual measured PSF for an "L" active area shaped pixel. The lighter the tint - the stronger the response.

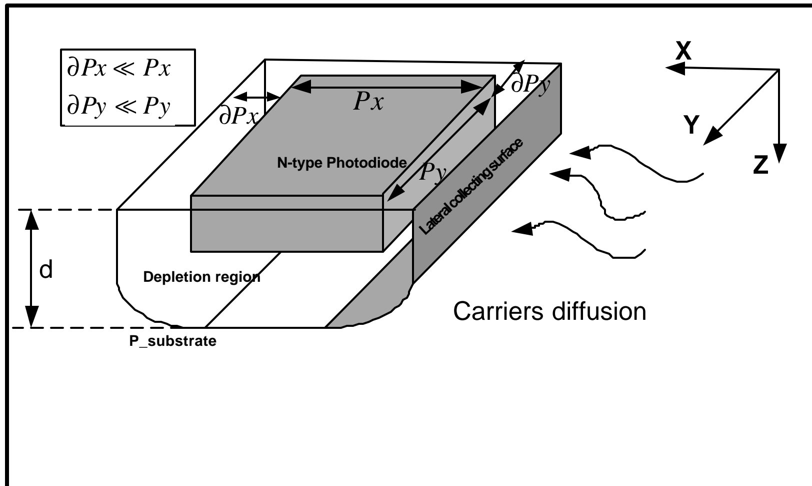

Fig. 6: The side - wall or lateral collecting surface, built up from the junction bottom and side - wall depletion capacitances. Here $P[mm]$ -is the photodiode perimeter, Px; Py - its dimensions in X and Y directions correspondingly, and $d\,[mm]$ -is the junction depth. ∂Px; ∂Py - are the lateral depletion stretches.

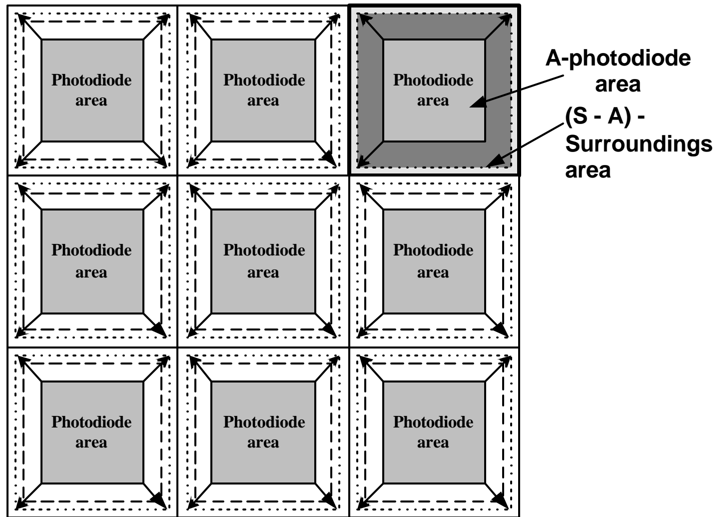

Fig. 7: A schematic illustration of the situation where the active area increases and reaches the pixel boundary (i.e., $A = S$, for all the pixels in array). As a result of the photodiode area extension the diffusion contribution eq uals zero.

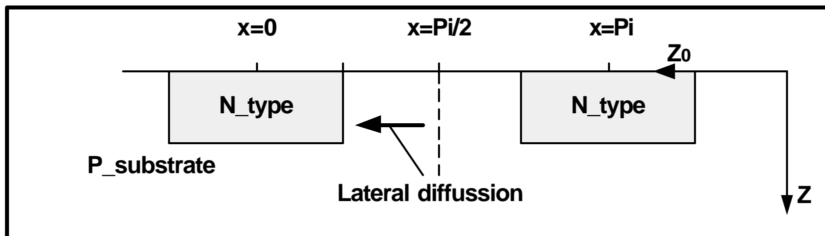

Fig. 8: A schematic cross section of several imager sites, which illustrates the diffusion distance dependence on the photodiode geometry. Here, Pi –is pixel pitch.

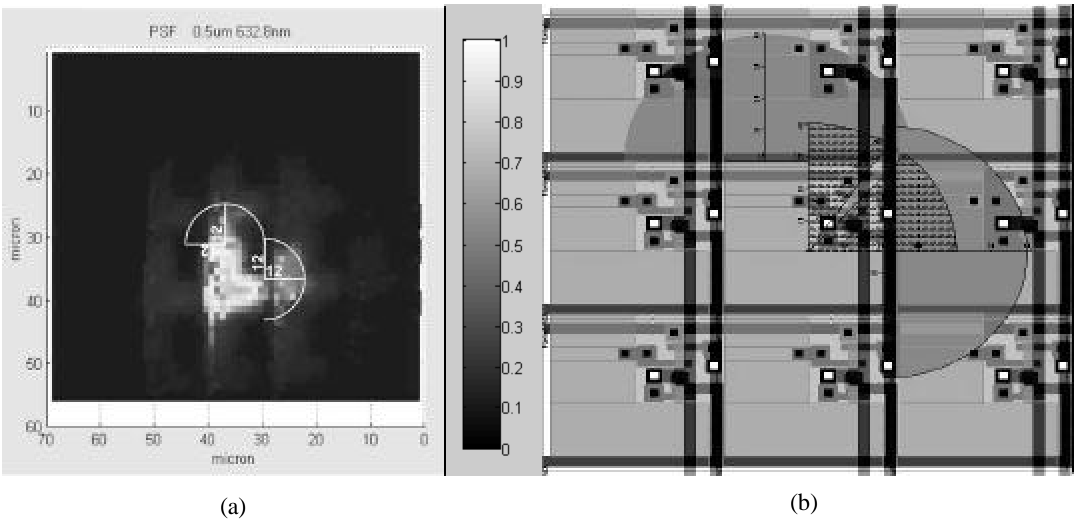

(a) (b)

Fig. 9. (a) Indicates the distance from the depletion boundary where the signal value reduces as 1/3e from its maximum value in the central pixel, (b) Represents the corresponding layout with the indication of the enclosed areas.